Cellulose (2026) 33:1001–1021
https://doi.org/10.1007/s10570-025-06907-y

ORIGINAL RESEARCH

Bacterial nanocellulose biohybrid membranes and beads for potential cosmetics, food, and drug delivery applications

Kaja Kupnik · Neža Brezovec · Željko Knez · Maja Leitgeb · Mateja Primožič

Received: 16 July 2025 / Accepted: 14 December 2025 / Published online: 8 January 2026

Abstract Bacterial nanocellulose is a promising biomaterial extensively used in functional foods and for drug delivery. Moreover, its characteristics can further be potentialized whether coupled with natural bio-extracts to endow antibacterial activity. *Persea americana* or avocado seed extracts are rich in phytochemicals and have demonstrated their antioxidant, antimicrobial and enzymatic activities, therefore encapsulating them into bacterial nanocellulose (BNC) may offer a potential release system of antibacterial avocado seed compounds. Accordingly, this study explores the in-depth insight into the influence of different bacterial nanocellulose producing strains (*Komagataeibacter hansenii* and *Komagataeibacter xylinus*) and cultivation conditions (static and dynamic cultivation, fermentation time) on the bacterial nanocellulose productivity and characteristics. The obtained bacterial nanocellulose membranes and beads were characterized in terms of chemical structure, morphology and crystallinity. More profitable and productive *K. xylinus* was further selected for encapsulation (up to 72.89 mg) of avocado seed extracts into bacterial nanocellulose membranes and beads in order to comprehensively evaluate the kinetic release profiles and determine their antibacterial activity against *Escherichia coli* and *Staphylococcus aureus.* Results of the study show that the bacterial nanocellulose and avocado seed extracts biohybrids represent a promising immediate (up to 17.39 mg in 1 h) and sustained (up to 35.04 mg in 48 h) release systems. Kinetic release modeling and cytotoxicity assessments confirmed controlled release behavior and biocompatibility for safe antibacterial applications in cosmetics, functional foods and drug delivery.

Keywords Bacterial nanocellulose beads · Avocado seed extract · Re-hydration · Release · Antibacterial activity

K. Kupnik · Ž. Knez · M. Leitgeb · M. Primožič (✉)
Faculty of Chemistry and Chemical Engineering, University of Maribor, Smetanova Ulica 17, 2000 Maribor, Slovenia
e-mail: mateja.primozic@um.si

K. Kupnik
e-mail: kaja.kupnik@ftpo.eu

Ž. Knez
e-mail: zeljko.knez@um.si

M. Leitgeb
e-mail: maja.leitgeb@um.si

K. Kupnik
Faculty of Polymer Technology, Ozare 19, 2380 Slovenj Gradec, Slovenia

N. Brezovec
Department of Rheumatology, University Medical Centre Ljubljana, 1000 Ljubljana, Slovenia
e-mail: neza.brezovec@gmail.com

Ž. Knez · M. Leitgeb
Faculty of Medicine, University of Maribor, Taborska Ulica 8, 2000 Maribor, Slovenia

Introduction

High surface area and porosity are one of the main benefits of nanofibrous matrices which are favored as carriers for delivery and release of divergent therapeutic agents (Thakkar and Misra 2017; Kupnik et al. 2020). As the most prevalent biopolymer with a supramolecular fibrous morphology, cellulose is of particular interest. Its highly crystalline and pure form of bacterial nanocellulose (BNC) exhibits even greater potential, as it is generated in a biotechnological process by *Komagataeibacter* (i.e., *Gluconacetobacter*, *Acetobacter*) bacterial strains and due to its divergent production of various shapes (e.g., membranes, fleeces, beads, aggregates, tubes, …) (Klemm et al. 2011). Lately, BNC has been examined as a carrier for drug delivery of active ingredients and their release to a great extent. However, it is of interest to understand the release mechanisms, which are governed by different factors such as crystallinity, swelling properties, pore size distribution, specific surface area, and porosity (Adepu and Khandelwal 2020). *K. xylinus* and *K. hansenii* are one of the most efficient and studied species for biosynthesis of BNC, of which quality and characteristics are strongly dependent on the producer strain (Chen et al. 2019b). However, an important factor in terms of BNC productivity and its quality are the cultivation conditions. Up to now, especially BNC membranes (BNCMs) have gained more importance in commercial drug delivery, as they are produced by static cultivation with the possibility of expansion to mass production, which also enables obtaining BNCMs with high mechanical stability and a uniform surface with homogeneous nanofiber networks (Shavyrkina et al. 2021). Agitated cultivation enables obtaining BNC in the form of beads (BNCBs). The yield of agitated cultivation is usually lower than in static conditions because bacteria can mutate into strains that do not produce BNC, due to the shear forces present during the process itself (Lee et al. 2014).

In the available literature, BNCBs have been studied for drug delivery purposes using antibiotics to a small extent and they certainly represent a huge potential, as e.g. drug carriers in oral dosage forms (Pötzinger et al. 2017). To the best of our knowledge, there is only one recent study (Osorio et al. 2024) of BNC spheres with bio-extract from *Vaccinium meridionale swartz* for potential delivery purposes in the reviewed literature.

BNC is known as a material that is generally recognized as safe (GRAS) (Gama et al. 2016), and was already applied as functional foods (Fontana et al. 2017). However, the antimicrobial properties of the materials are extremely important for biomedical, cosmetic and pharmaceutical applications, which BNC itself lacks. Functional foods that consist of high amounts of bioactive compounds may provide desirable health benefits and could play an important role in prevention of various lifestyle-related diseases, such as diabetes, cancer, neurological and cardiovascular diseases (Konczak and Zhang 2004). The use of bio-extracts from plants is gaining scientific impetus and in our recent research (Kupnik et al. 2024), it was found that BNCMs from *K. hansenii*, modified with avocado seed extracts (ASE), represent an outstanding potential as antibacterial nanocellulose hybrids with a high degree of swelling and water retention, which maintain a suitable moist environment for applications in wound healing. For this purpose, the presented follow-up study was carried out, which provides an in-depth insight into the influence of different bacterial strains (*K. hansenii* and *K. xylinus*) and cultivation conditions (static and agitated cultivation, cultivation time, etc.) on the yield of produced BNCMs/BNCBs and their quality and characteristics, such as chemical structure, morphology, crystallinity and determination of the dominant crystalline allomorph. Therefore, the main objective of our research was to investigate the release and cytotoxicity of ASE from BNCMs/BNCBs and to evaluate the antibacterial effectiveness of obtained BNC biohybrids against Gram-negative (G-) bacteria *E. coli* and Gram-positive (G+) bacteria *S. aureus*.

The reason for the selection of ASE is their exceptional antimicrobial, enzymatic and antioxidant efficiency. ASE contain a complex array of bioactive compounds including phenolic acids (e.g., chlorogenic, caffeic, ferulic, gallic), flavonoids (e.g., epicatechin, hesperidin, quercetin), proanthocyanidins, and lipophilic acetogenins (e.g., avocadene, persin, persediene, persenone A-C). The antimicrobial activity is primarily mediated by phenolic compounds that disrupt bacterial membrane permeability and inhibit metabolic enzymes, while acetogenins and fatty acids intercalate into phospholipid bilayers, compromising membrane integrity and causing cellular lysis through

increased fluidity and loss of electrochemical gradients (Kupnik et al. 2023). Additionally, the very use of waste biomass, i.e. inedible avocado seeds, enables the potential towards the circular economy and the utilization of "garbage" for sustainable products with added value. Such biohybrids show potential as a sustainable alternative to BNC hybrids with encapsulated synthetic antibiotics, as due to the exceptional bioactivity of ASE, they could be applied preventively as functional food or in cosmetics, while simultaneously providing effective delivery of antibacterial avocado seed compounds.

Our research uniquely optimizes BNC biosynthesis for both BNCMs and innovative BNCBs while establishing a novel and sustainable BNC biohybrid platform utilizing ASE from waste biomass. Through comprehensive release kinetic modeling and cytotoxicity assessments, this study demonstrates controlled bioactive compound delivery with confirmed biocompatibility, representing a systematic and scalable approach for integrating divergent natural extracts from various waste sources. This advancement offers significant potential for safe applications in cosmetics, functional food, and drug delivery while marking substantial improvement over existing fragmented research approaches.

Experimental

Chemicals and microorganisms

Acetic acid (glacial, ≥ 99.7%), agar, sodium hydroxide (NaOH, ≥ 95.0%), sucrose, and yeast extract were purchased from Sigma-Aldrich, St. Louis, USA, while citric acid (≥ 99.5%), D-(+)-glucose anhydrous (≥ 97.5%), di-sodium hydrogen phosphate (Na_2HPO_4, ≥ 99.0%), ethanol (EtOH, ≥ 99.5%), and peptone were obtained from Merck, Darmstadt, Germany. Hydrochloric acid (HCl, ≥ 99.8%) and sodium hydroxide (NaOH, ≥ 99.8%) were purchased from Honeywell Fluka, North Carolina, United States, while the Mueller–Hinton broth was from Biolife, Milano, Italy. All chemicals were used without further purification.

The selected microorganisms (*K. hansenii* (DSM 5602), *K. xylinus* (DSM 2325), *E. coli* (DSM 498), and *S. aureus* (DSM 346)) were purchased from DSMZ-German Collection of Microorganisms and Cell Cultures GmbH from Berlin, Germany.

Production of BNCMs/BNCBs

BNC was obtained by culturing *K. hansenii* and *K. xylinus* producer strains, which was carried out at 26 ± 1 °C. For the *K. xylinus,* the complex Hestrin and Schramm (HS) medium (Urbina et al. 2021) was selected as the growth and production medium, with a standard composition of 2.0% (w/v) glucose, 0.5% (w/v) peptone, 0.5% (w/v) yeast extract, 0.115% (w/v) citric acid and 0.27% (w/v) Na_2HPO_4. Prior to sterilization at 121 ± 1 °C, the pH value of the medium was adjusted to 6.0 using HCl or NaOH, respectively. According to our previous study (Kupnik et al. 2024), optimized composition of production medium for *K. hansenii* was adopted.

One loopful of selected acetic acid bacteria was inoculated in 50 mL of growth HS medium, and grown at 26 ± 1 °C on a rotary shaker (120 rpm) for 24 h. The obtained suspension was used as an inoculum (2, 5, and 10% (v/v), $1–5 \times 10^6$ CFU/mL). The inoculated flasks were incubated under static and dynamic (60, 120, and 180 rpm) conditions at 26 ± 1 °C in order to produce BNCMs/BNCBs. After cultivation and production of at least 3 days for *K. xylinus* and 17–21 days for *K. hansenii*, the prepared BNCMs/BNCBs were separated by filtration, rinsed thoroughly with distilled water, and immersed in 1 M NaOH solution for at least 24 h to remove the bacterial cells and residual nutrient components embedded in the harvested BNC. Finally, the BNCMs/BNCBs were purified again with distilled water until the neutral pH stabilized.

X-ray diffraction analysis of the BNCMs/BNCBs

The crystallinity of the BNCMs/BNCBs was characterized by X-Ray Diffraction (XRD) using a Bruker D2 Phaser (MA, USA) diffractometer with Cu Kα radiation (λ = 1.54 Å) at 30 kV and 10 mA. Scattered radiation was detected at a scan rate of 0.3 s/step in the range of 2θ from 5 to 70°. The crystallinity index (C_I) was calculated using the Eq. 1, developed by Segal et al. (1959):

$$C_I[\%] = \frac{I_{110} - I_{AM}}{I_{110}} \times 100 \quad (1)$$

where I_{AM} and I_{110} are the minimum in the diffraction intensity between the 010 and 110 peaks at $\approx$ 18° 2θ related to the amorphous regions in the cellulose, and the intensity of the diffraction peak at 2θ = 22.7° related to the (110) diffraction plane of cellulose I_α (French and Santiago Cintrón 2013; French 2014; Singhsa et al. 2018). The d-spacing calculations of BNC samples were performed using Bragg's Eq. 2:

$$d[nm] = \frac{n\lambda}{2\sin\theta} \quad (2)$$

where n represents the diffraction order, λ corresponds to the X-ray wavelength (0.154 nm), and θ indicates the Bragg diffraction angle for the specific crystallographic plane. To identify the predominant polymorphic form (I_α or I_β) present in various BNCM specimens, the methodology developed by Wada and colleagues (Wada et al. 2001) was employed. This calculation (Eq. 3) introduces a function designed to distinguish between I_α-dominant and I_β-dominant crystalline structures:

$$Z = 1693d_1 - 902d_2 - 549 \quad (3)$$

where the parameters d_1 and d_2 represent the interplanar spacings for the (100) and (010) crystallographic planes of the I_α unit cell, respectively. When the calculated value Z exceeds zero, the BNCM sample is categorized as I_α-predominant, whereas negative Z values signify I_β-predominant characteristics.

Ultrasound assisted extraction of avocado seeds

The ASE from *Persea americana* (Hass variety) was prepared by ultrasound assisted extraction (UE), using water as a solvent, as detailed in our publication (Kupnik et al. 2023). The obtained UE ASE was stored at -20 ± 1 °C before its further usage.

Modification of the BNCMs/BNCBs with UE ASE

For modification of the BNCMs/BNCBs from *K. xylinus*, the UE ASE was dispersed individually in sterilized deionized water (dH_2O), to prepare 10 wt% concentrated UE ASE solution. The exhaust method (Sakthivel et al. 2016; Sharma and Bhardwaj 2019) was applied and the wet or freeze-dried BNCMs/BNCBs were immersed in UE ASE solution at room temperature for 48 h. The magnetic stirrer of 100 rpm was used to facilitate diffusion of the UE ASE into the BNCMs/BNCBs. After adsorption, the modified BNCMs/BNCBs were taken out and soaked over a filter paper to remove the excess extract.

Chemical and morphological characterization of BNCMs/BNCBs

Chemical characterization of pure and modified BNCMs/BNCBs was performed using Attenuated Total Reflectance–Fourier Transform Infrared (ATR-FTIR). For recording the spectrum, whole freeze-dried BNCBs were used, while for BNCMs, approx. 1 cm^2 freeze-dried pieces were used. The IR spectra was recorded using a Perkin-Elmer spectrum one FTIR spectrometer (Waltham, MA, USA) with ATR crystal accessories at ambient conditions, from collecting 16 scans per spectrum and a 4 cm^{-1} resolution for each sample at a region of 4000–400 cm^{-1}. The background and air spectrum subtraction were performed in parallel. For the data analysis, The Spectrum 5.0.2 software was used.

The morphology of freeze-dried BNCMs/BNCBs was examined by a high-resolution Scanning Electron Microscopes (SEM), FEI Sirion 400 NC and FEI Quanta 200 3D (FEI, Hillsboro, OR, USA). The BNCBs or approx.1 cm^2 pieces of BNCMs were cut, placed on a holder and sputtered with carbon to ensure conductivity and prevent charging effects. Additionally, BNCMs/BNCBs were observed under Stereomicroscope System SZX10 equipped with Olympus EP50 camera (Evident, Tokyo, Japan) to obtain a high-quality 3D image of samples. Fiber diameters of BNCMs were measured using ImageJ software (n = 10 fibers) from high-magnification SEM images, focusing on distinguishable individual fibers at membrane edges and surfaces.

Release of UE ASE from BNCMs/BNCBs

In order to determine the release of UE ASE from the BNCMs/BNCBs from *K. xylinus*, wet and freeze-dried BNCBs (in diameter of approx. 2 (S), 5 (M), and 7 (L) mm) or BNCMs (in size of approx. 1 cm^2) with encapsulated UE ASE were placed in a vial containing 5 mL of PBS (0.1 M, pH 7.4) at 37 ± 1 °C

with constant stirring (100 rpm). After specific time periods (0.5, 1, 2, 3, 4, 24, and 48 h), the samples were collected, and the same volume of fresh PBS was replaced. The release of UE ASE was monitored spectrophotometrically at λ_{max} of 280 nm. The concentration (mg/mL) of released UE ASE was determined using pre-prepared calibration curve for UE ASE. Percentage release (%) of the UE ASE was calculated using the following Eq. 4:

$$Release[\%] = \frac{released\ concentration\ of\ UE\ ASE\ at\ a\ specific\ time}{incorporated\ concentration\ of\ UE\ ASE\ in\ BNCB/BNCM} \times 100 \quad (4)$$

All the experiments were performed in triplicates, and results are presented as the mean value ± SD.

The release kinetics of UE ASE from BNCMs/BNCBs in PBS were evaluated using selected mathematical models using data analysis and graphing software OriginPro® (OriginLab Corporation, Northamptom, MA, USA). Selected models encompass the zero-order model, depicting the constant rate of substance released over time, the first-order model, showing a logarithmic correlation between the remaining substance percentage and time, and the Korsmeyer-Peppas model, illustrating the logarithmic relationship between the percentage of substance released and time (Kučuk et al. 2024).

Antibacterial activity of BNCMs/BNCBs enriched with UE ASE

To qualitatively assess the antibacterial activity against *E. coli* and *S. aureus* of the *K. xylinus* BNCMs/BNCBs with incorporated UE ASE, the agar diffusion assay was applied, following the protocol described in our previous study (Kupnik et al. 2024). The unmodified BNCMs/BNCBs were used as negative controls. The results are reported as mm of the inhibition zone and are presented as the mean value ± SD, as the experiments were performed in triplicates.

Cytotoxicity evaluation

Cytotoxicity was assessed using the EZ4U Nonradioactive Cell Proliferation and Cytotoxicity Assay, Cat. No. BI-500 (Biomedica Medizinprodukte GmbH, Wien, Austria) according to the manufacturer's instructions. The extract was initially dissolved in water and subsequently diluted in RPMI 1640 cell culture medium (Stemcell) supplemented with 2 mM L-Glutamine, to achieve final concentrations of 300, 100, 30, 10, and 1 µg/mL. THP-1 human monocytic cells were seeded into a 96-well plate at a density of 3×10^3 cells per well and treated with the different extract dilutions. Untreated cells, receiving an equal volume of medium, served as the control group. The cells were incubated for 24 h in a humidified incubator at 37 °C with 5% CO_2. Following incubation, 20 µL of the substrate solution was added to each well, and the plate was incubated for an additional 4 h. Absorbance was measured using a microplate reader at 450 nm, with a reference wavelength of 620 nm. The experiment was performed in triplicate.

Statistical analysis

Statistical analyses were performed using IBM® SPSS® Statistic. Normality was assessed using Shapiro–Wilk tests and homogeneity of variances using Levene's test. For normally distributed data with equal variances, one-way ANOVA followed by Tukey HSD post-hoc tests were employed. For data violating parametric assumptions, Kruskal–Wallis tests with Dunn's post-hoc comparisons were used. Statistical significance was set at $\alpha = 0.05$. Compact letter displays were generated to indicate statistically homogeneous groups.

Figure 1 depicts the comprehensive experimental workflow, illustrating the parallel production of bacterial nanocellulose and avocado seed extract preparation, followed by biohybrid modification and subsequent characterization through structural, morphological, release kinetic, and biological activity assessments.

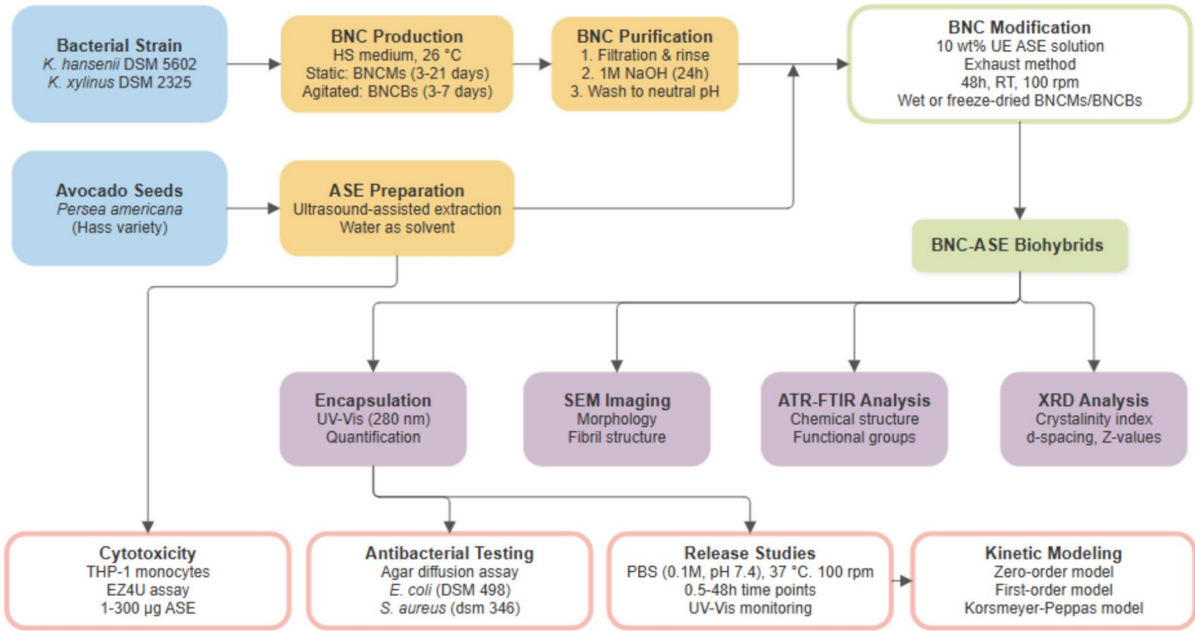

Fig. 1 Experimental flow chart

Results and discussion

Productivity, chemical structure, morphology and crystallinity of BNCMs from K. hansenii and K. xylinus

It is well known that the production of BNC varies with the strains and cultivation conditions, therefore *K. hansenii* and *K. xylinus* were selected for comparison of its BNC productivity. In static cultivation, *K. hansenii* and *K. xylinus* resulted as good producers of BNCMs. An extremely important fact is that *K. hansenii* takes an average of 17–21 days to produce BNCM, while *K. xylinus* produces BNCM in just 3 days. According to our already conducted optimization study of *K. hansenii* cultivation and yield itself (Kupnik et al. 2024), the research in this study on BNC productivity focused more on *K. xylinus*, which with a shorter production time enables faster BNC recovery and reduction of production costs. The productivity results of BNCMs from *K. xylinus* are shown on Fig. 2. It was found that after only 3 days of fermentation, extremely compact BNCMs were formed, the mass of which increased up to 7 days and reached an average of 10.0 ± 1.5 g. On the 10th day of fermentation, two BNCMs were already present in the Erlenmeyer flask, and their total mass had more than doubled and amounted to an average of 24.3 ± 2.8 g. The appearance of the new BNCM is a fairly known step in the fermentation process and is the result of the submergence of the BNCM, which was formed previously, due to its mass and thickness. Since the nutritional value in the cultivation medium is still sufficiently high, the formation of new cellulose fibers can begin at the surface-air interface, which arise from linearly arranged pores on the surface of the bacteria. This is followed by the process of cellulose fibers crystallization into micro/nano fibrils and the further formation of intertwined cellulose ribbons that form BNCM (Wang et al. 2019).

Interestingly, after 70 days of cultivation in the starting medium, without any subsequent addition of nutrients to the medium, four BNCMs were present in the Erlenmeyer flask, and after 100 days as many as seven BNCMs (Fig. 2c), with the mass of 54.1 ± 2.4 g and 64.8 ± 3.1 g, respectively. Statistical analysis confirmed that culture time significantly affected membrane mass production ($p < 0.001$), with extended cultivation periods (70–100 days) yielding significantly higher masses compared to all earlier time points ($p < 0.001$). Here it is necessary to highlight the extremely high productivity

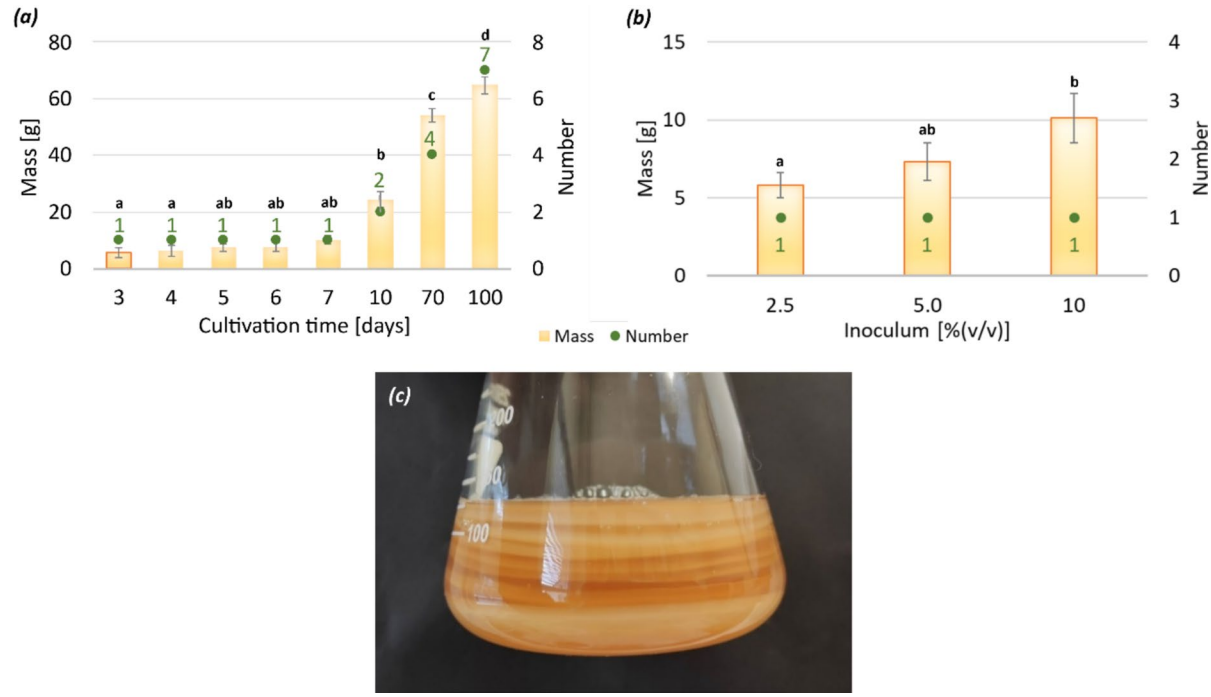

Fig. 2 Mass (column) and number (dot) of formed BNCMs in relation to **a** cultivation time (5% (v/v) of inoculum) and **b** volume of inoculum (after 3 cultivation days) of *K. xylinus* in HS medium at 26 ± 1 °C. **c** visual appearance of 7 BNCMs after 100 days of cultivation. Different letters above each column denote significant differences ($p < 0.05$) in mass of formed BNCMs

of *K. xylinus* compared to *K. hansenii*, which after 21 days produced one BNCM with a weight of 6.3 ± 0.8 g, after 28 days two BNCMs with a weight of 9.6 ± 0.7 g and after 35 days three BNCMs with a mass of 11.8 ± 1.7 g (Kupnik et al. 2024). The productivity of *K. hansenii* was 117.8 g/L after 35 days, while *K. xylinus* produced BNCMs after 3 days with 44.8 g/L, after 10 days 194 g/L, and 100 days as much as 518.4 g/L. As expected, increasing the added volume of the inoculum (Fig. 2b) also increased the mass and yield of BNCMs. With the addition of 10% (v/v) inoculum, the mass of the obtained BNCM increased to 10.1 ± 1.6 g (81.0 g/L) after only 3 days of cultivation.

Hereafter, the characterization of BNCMs produced by *K. hansenii* and *K. xylinus* was performed. First, FTIR analysis (Fig. 3a) of both freeze-dried BNCMs were carried out in order to gain insight into their chemical composition. Both spectra exhibited characteristic absorption bands dominated by type-I cellulose (i.e. peaks for O–H stretching vibrations around 3350 cm^{-1}, C–H and asymmetric CH_2 stretching at 2890 cm^{-1}, deformational vibrations of OH groups of bound water around 1640 cm^{-1}, symmetrical bending of CH_2 groups at 1428 cm^{-1}, stretching C–O–C and C–O vibrations correspond to peaks in the region of 1200–1000 cm^{-1}, β-1,4 bonds vibrations are characterized by peak around 850 cm^{-1} (Ghozali et al. 2021)), but differ most in the range between 1500–1200 cm^{-1}, which is extremely sensitive to molecular and chemical structural transformations (Atykyan et al. 2020). The FTIR spectrum of BNCM from *K. hansenii* showed an extremely intense peak at 1428 cm^{-1}, which represents the bending of CH_2 groups and is one of the main peaks of cellulose I_α allomorph (Gayathri and Srinikethan 2019). Furthermore, BNCM from *K. xylinus* exhibited more intense peaks at 1374, 1337 and 1315 cm^{-1}, which correspond to bending of the C–H, O–H, and CH_2 groups, indicating the presence of crystalline regions within the BNCMs structure (Osorio et al. 2020). With approaching the area of spectra between 780 and 680 cm^{-1}, the 750 and

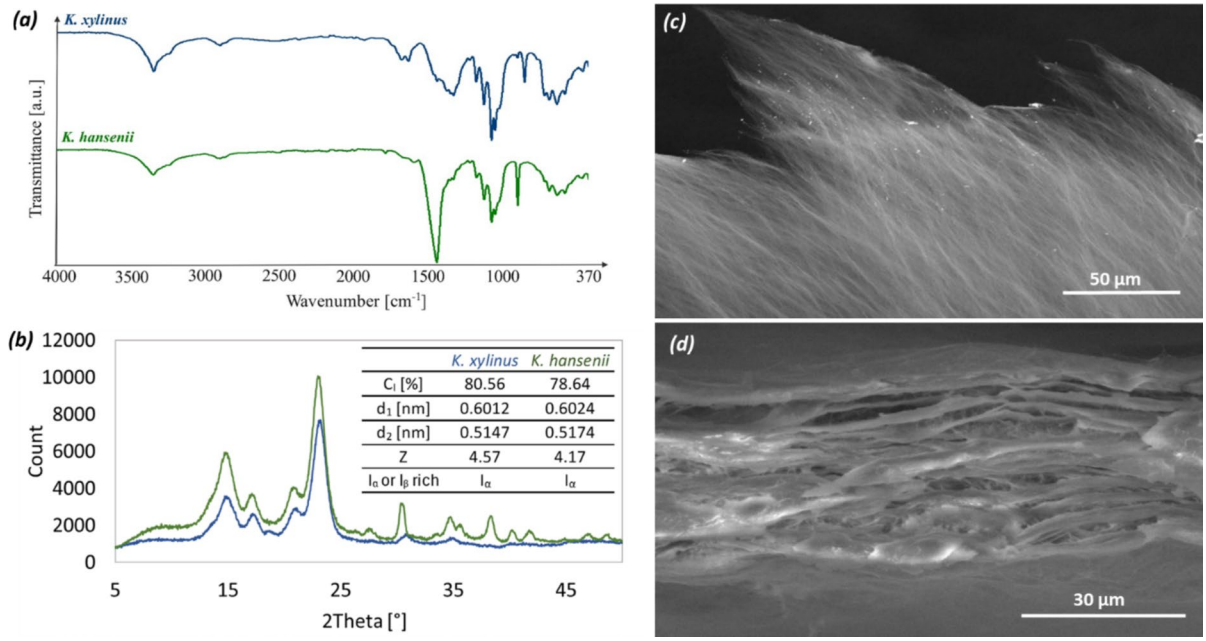

Fig. 3 **a** ATR-FTIR spectra and **b** XRD patterns with crystallinity index (C_I), d-spacing and Z values for freeze-dried BNCMs from *K. xylinus* (HS medium, 3 days at 26 ± 1 °C, 5% (v/v) of inoculum) and *K. hansenii* (modified HS medium, 21 days at 26 ± 1 °C, 5% (v/v) of inoculum) and SEM micrographs of **c** surface (voltage 15.0 kV, magnification 1000x) and **d** cross-section (voltage 15.0 kV, magnification 2500x) of BNCM from *K. xylinus* (HS medium, 3 days at 26 ± 1 °C, 5% (v/v) of inoculum)

710 cm^{-1} peaks were observed, indicating the presence of crystalline allomorphs I_α and I_β.

Regarding the crystallinity of BNCMs from *K. hansenii* and *K. xylinus*, the XRD diffractograms presented in Fig. 3b confirmed the semi-crystalline structure of cellulose I, composed of crystalline and amorphous regions from allomorphs I_α and I_β (Atalla and VanderHart 1984). Both XRD patterns of the biosynthesized BNCMs interpret three main diffraction signals corresponding to cellulose I_α one-chain triclinic unit cell at $2\theta \approx 14.6$, 16.8, and 22.7° with Miller indices of (100), (010), and (110), which concur with the peaks $(1\bar{1}0)$, (110), and (200) of cellulose I_β (French 2014). Additional diffraction signal at $2\theta \approx 20.5°$ belongs to several overlapping I_α crystalline signals $(11\bar{2})$, $(01\bar{2})$, and $(10\bar{2})$ (Heydorn et al. 2023). As we reported in our recent study (Kupnik et al. 2024), in some cases of BNCMs from *K. hansenii*, some additional peaks appeared, which are not from cellulosic material and may appear on the XRD pattern due to not efficiently purified BNCM and thus represent possible components of the nutrient medium. While these peaks, attributed to residual nutrient medium components following purification, do not interfere with the identification of the primary cellulose crystalline structure, they represent impurities that make it difficult to evaluate how they might influence drug delivery applications. Based on the reviewed literature (Digel et al. 2023), the cellulose produced from bacteria is mainly enriched with I_α crystalline allomorph. Therefore, in order to evaluate the dominant classification of the allomorphs I_α and I_β, the d-spacing and Z values were calculated based on a methodology by Wada and colleagues (Wada et al. 2001). Results indicated the domination of I_α type (triclinic structure, $Z > 0$) for both BNCMs from different producing strains, regarding the Z values of 4.17 and 4.57 for *K. hansenii* and *K. xylinus*, respectively. Additionally calculated crystallinity index (C_I) of BNCMs resulted in 78.64% for *K. hansenii* and 80.56% for *K. xylinus* BNCMs, which also coincides with the fact that the higher the crystallinity, the higher the Z value, confirming the higher proportion of the triclinic structure in BNCMs. Here it is necessary to accentuate that the crystallinity is highly dependent on the BNC producing bacterial strain,

nutritional composition of media and cultivation time (Dayal et al. 2013). The crystallinity of BNC for different *Komagataeibacter* spp. ranged from 64 to 80% (Vigentini et al. 2019; Gupte et al. 2021), which coincides with the presented results.

Furthermore, the BNCMs microstructures were observed using SEM imaging. There was no significant difference between the BNCMs produced using different bacterial strains. The surface and the cross-section of the *K. xylinus* are presented in Fig. 3c and Fig. 3d, respectively.

The surface image (Fig. 3c) reveals perfect fibrillar organization, where each fibril is comprised of single linear cellulose chains forming a compact net. At the same time, the cross-section image (Fig. 3d) depicts layered, plate-like fibrillated structure with a well-oriented and open microporous network, due to the freeze-drying method. The diameters of the fibers ranged from 60 to 120 nm, which is in accordance with the results in the literature (Manoukian et al. 2019; Gayathri and Srinikethan 2019).

Productivity, chemical structure and morphology BNCBs from K. xylinus

Figure 4 illustrates the results related to *K. xylinus* BNCBs production in agitated culture with varying parameters and their effects on the final productivity. Since the formation of nanocellulose fibers and the productivity of *K. hansenii* is slower and lower and the BNCBs were thus not formed, only *K. xylinus* was employed for the formation of BNCBs.

Initially, the effect of cultivation time (Fig. 4a) on the mass, number and diameter of BNCBs was evaluated. It was found that, like BNCMs, BNCBs are formed after 3 days of cultivation, and the number of beads in the Erlenmeyer flask itself did not increase with additional days of cultivation. On the contrary, the mass and diameter of the BNCBs increased with additional days of cultivation. Based on the literature (Wu and Lia 2008; Mohite and Patil 2014; Lazarini et al. 2022), an initial shaking speed of 120 rpm was selected. After 3 days of cultivation, an average of 12 ± 3 BNCBs were formed in Erlenmeyer flasks, with a total mass of 2.9 ± 0.6 g and an average diameter of 7.2 ± 0.4 mm, while after 7 days of cultivation, the mass increased by almost 2 times and resulted in 5.1 ± 0.7 g and diameters 8.4 ± 0.6 mm. Culture time significantly affected bead mass production ($p < 0.001$), with day 7 beads weighing 77.9% more than day 3 beads ($p < 0.001$).

As expected, increasing the added volume of the inoculum (Fig. 4b) also increased the total mass and number of produced BNCBs, due to the higher concentration of nanocellulose-producing bacterial cells present in culture medium. However, the diameter of the BNCBs remained the same, since with the same shaking conditions (120 rpm) the process of combining nanocellulose fibers into BNCBs did not change. Statistical analysis confirmed a significant effect of inoculum volume on bead mass ($p = 0.002$), with the addition of 10% (v/v) inoculum, the mass of 18 ± 2 BNCBs increased to 9.6 ± 1.2 g (76.8 g/L) after only 3 days of cultivation. Changing the agitated conditions can have a tremendous impact on the formation, mass, diameter and number of BNCBs. Therefore, an insight into three different agitation speeds (180, 120, 60 rpm) was performed after 3 (Fig. 4c1) and 7 (Fig. 4c2) days of *K. xylinus* cultivation. It was observed that with the lowest shaking speed (60 rpm) after 3 days of fermentation, only one large (30.3 ± 2.8 mm) BNCB with a mass of 6.4 ± 0.6 g was formed. By increasing the shaking speed to 120 rpm, an average of 12 ± 2 BNCBs with a total mass of 8.7 ± 0.9 g and a diameter of 7.3 ± 1.3 mm were obtained. An additional increase in the shaking speed to 180 rpm resulted in countless extremely small (2 ± 0.1 mm) BNCBs with a total mass of 11.3 ± 1.4 g. On day 3, higher shaking speeds significantly enhanced bead mass production ($p < 0.001$). Thus, the productivity of *K. xylinus* increased with increasing shaking speed after 3 days of cultivation, while the trend reversed after 7 days of cultivation. The mass of one formed BNCB at 60 rpm jumped by 4.3 times to 27.4 ± 1.3 g, and its diameter also doubled to 60.5 ± 4.9 mm. At 120 rpm, the mass of 12 ± 2 BNCBs increased by only 1.8 times (15.3 ± 1.6 g), as well as their diameter, which increased by 1.1 times (8.1 ± 1.6 mm). The diameter of the BNCBs at 180 rpm remained the same, while the mass gain after 7 days was only additional 2.9 g. This reversal was statistically significant ($p < 0.001$), with low agitation (60 rpm) producing 93% more mass than high agitation (180 rpm, $p < 0.001$) by day 7, while 120 and 180 rpm showed no significant difference ($p > 0.05$). When applying low agitation speed (60 rpm), the productivity is lower at the beginning due to a relatively low oxygen transfer, but

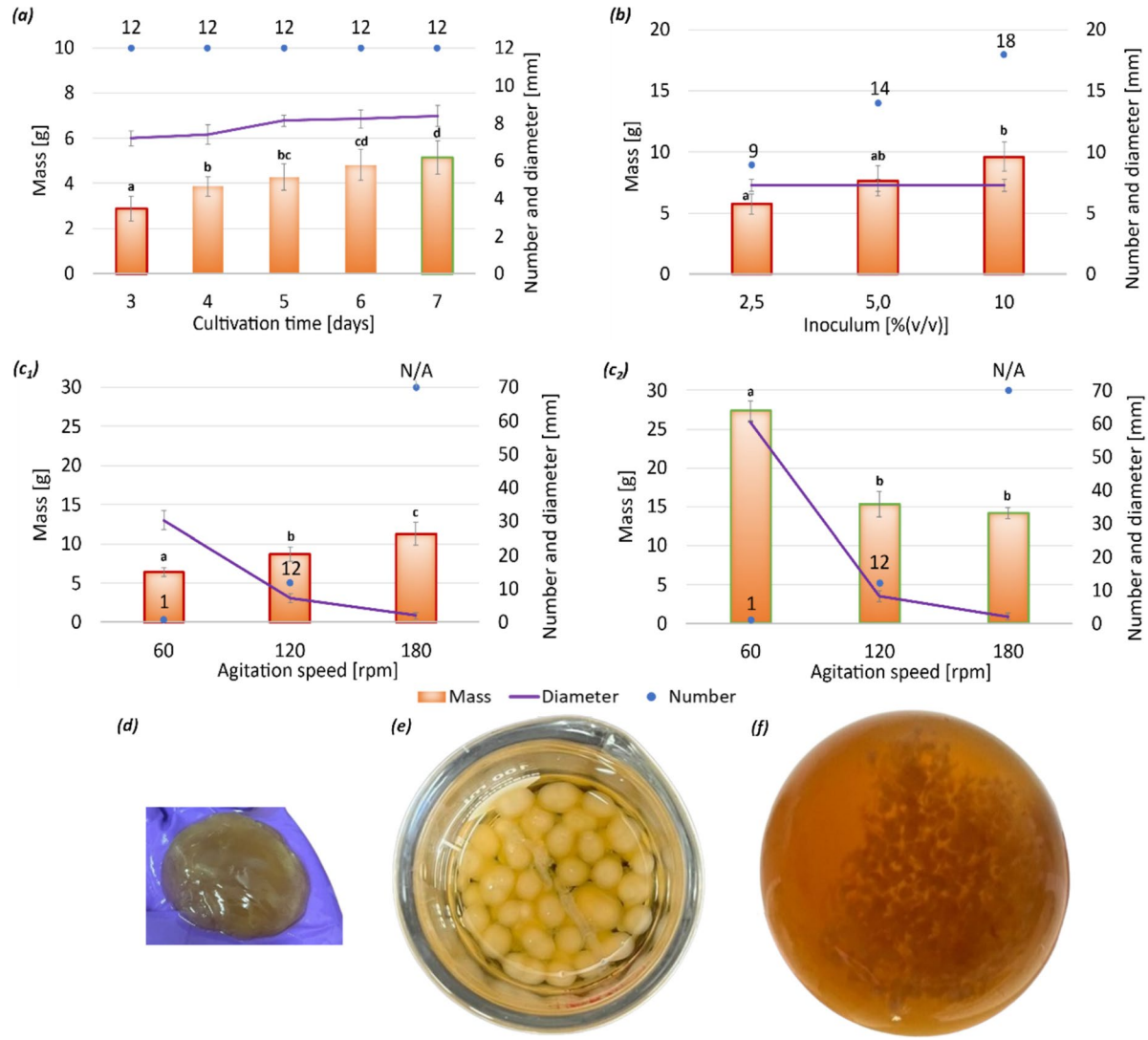

Fig. 4 Mass (column), diameter (line) and number (dot) of formed BNCBs in relation to **a** cultivation time (5% (v/v) of inoculum), **b** volume of inoculum (after 3 cultivation days), and **c** agitation speed (c_1 after 3 cultivation days, c_2 after 7 cultivation days) with visual appearance of unpurified BNCBs of *K. xylinus* obtained at **d** 60, **e** 120 and **f** 180 rpm in HS medium at 26 ± 1 °C after 7 days of cultivation. Different letters above each column denote significant differences ($p < 0.05$) in mass of formed BNCBs

it increases later due to the higher glucose contents present in the medium and its sustainable consumption (Chen et al. 2019a). The reduced productivity at higher agitation speeds (180 rpm) may be due to several reasons. A higher agitation speed can be used to obtain greater cellulose-producing bacterial cell density, as the higher speed offers increased aeration of the culture. Additionally, according to the literature (Chen et al. 2019a), at high speeds, glucose is consumed rapidly in the first 2 days, and as a result, the productivity is the highest in the first few days. Bae and colleagues (Bae et al. 2004) suggested that high agitation speeds cause high shear forces, causing bacteria to mutate and therefore produce less BNCBs. The lower BNCBs yield at 180 rpm compared to 100 and 60 rpm could also be due to the higher dissolved oxygen content, which increases the accumulation of the by-product gluconic acid, a metabolite of glucose,

resulting in the reduced nanocellulose production (Tantratian et al. 2005).

Figure 5 shows the appearance and structure of wet (Fig. 5a) and freeze-dried (Fig. 5b) native BNCBs. The SEM graphs (Fig. 5c and Fig. 5d) of BNCBs proved their porous and loose morphology, due to freeze-drying method. They showed a reticulated three-dimensional structure consisting of ultrafine cellulose nanofibrils. The fibril diameter of the BNCBs from the shaking cultivation was within the range of 30–120 nm. Here it is important to note that methods of drying BNC impact the morphology of the fibrillar network (Hu et al. 2014).

Chemical and morphological characteristics of BNCMs/BNCBs with incorporated UE ASE

Figure 6a-c shows the macroscopic appearance of wet and freeze-dried *K. xylinus* BNCBs and wet BNCM with incorporated UE ASE. Due to the presence of polyphenols and perseorangin in UE ASE (Dabas et al. 2011), a natural pigment from avocado seeds, the BNCMs/BNCBs present a vivid and bright orange-reddish colour. The visual appearance is very important if BNCMs/BNCBs biohybrids with UE ASE are intended for application as functional foods. For example, the BNC has already been used in the preparation of desserts when immersed in sugar syrup (Azeredo et al. 2019). For that reason, the sugar syrup could be replaced or supplemented with different ASE, which are rich in phytochemicals and exhibit exceptional antimicrobial properties (Kupnik et al. 2023).

According to the SEM micrograph (Fig. 6d-f) the BNCMs/BNCBs modified with UE ASE shows the rough structure, given by the interconnected network of nanocellulose fibrils. Nanofibrils are covered by the UE ASE particles, but still present an open porosity, which is crucial for the release of UE ASE. The UE ASE particles were randomly measured using ImageJ software, and their diameter ranged in between 1.3 and 2.5 µm, which is in line with the hydrodynamic size of the particles determined in our recent study (Kupnik et al. 2024).

The FTIR spectra of pure BNCB (Fig. 6g) represents the characteristics bands of cellulose type I allomorphism, already discussed before for the BNCMs FTIR spectra (see Fig. 3a and corresponding text). In the case of BNCB modified with UE ASE, the BNC and UE ASE bands are superimposed. However, there is still evidence of the presence of phytochemicals, confirming the incorporation of UE ASE in BNCB.

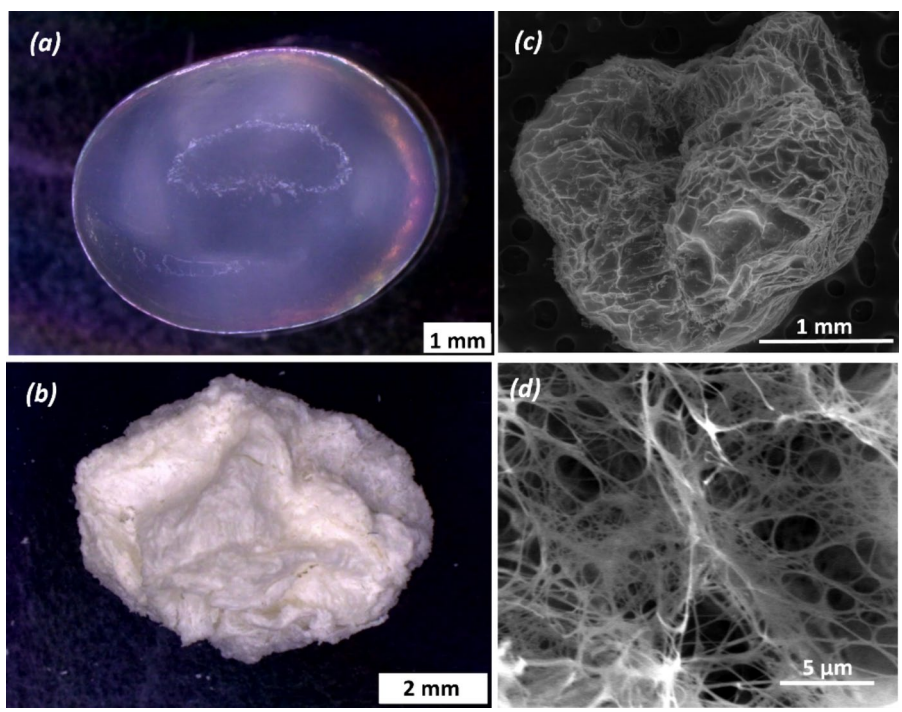

Fig. 5 Stereo microscopy imaging of **a** wet and **b** freeze-dried BNCBs with SEM micrographs of its **c** surface (voltage 15.0 kV, magnification 86x) and **d** inner structure (voltage 15.0 kV, magnification 10000x)

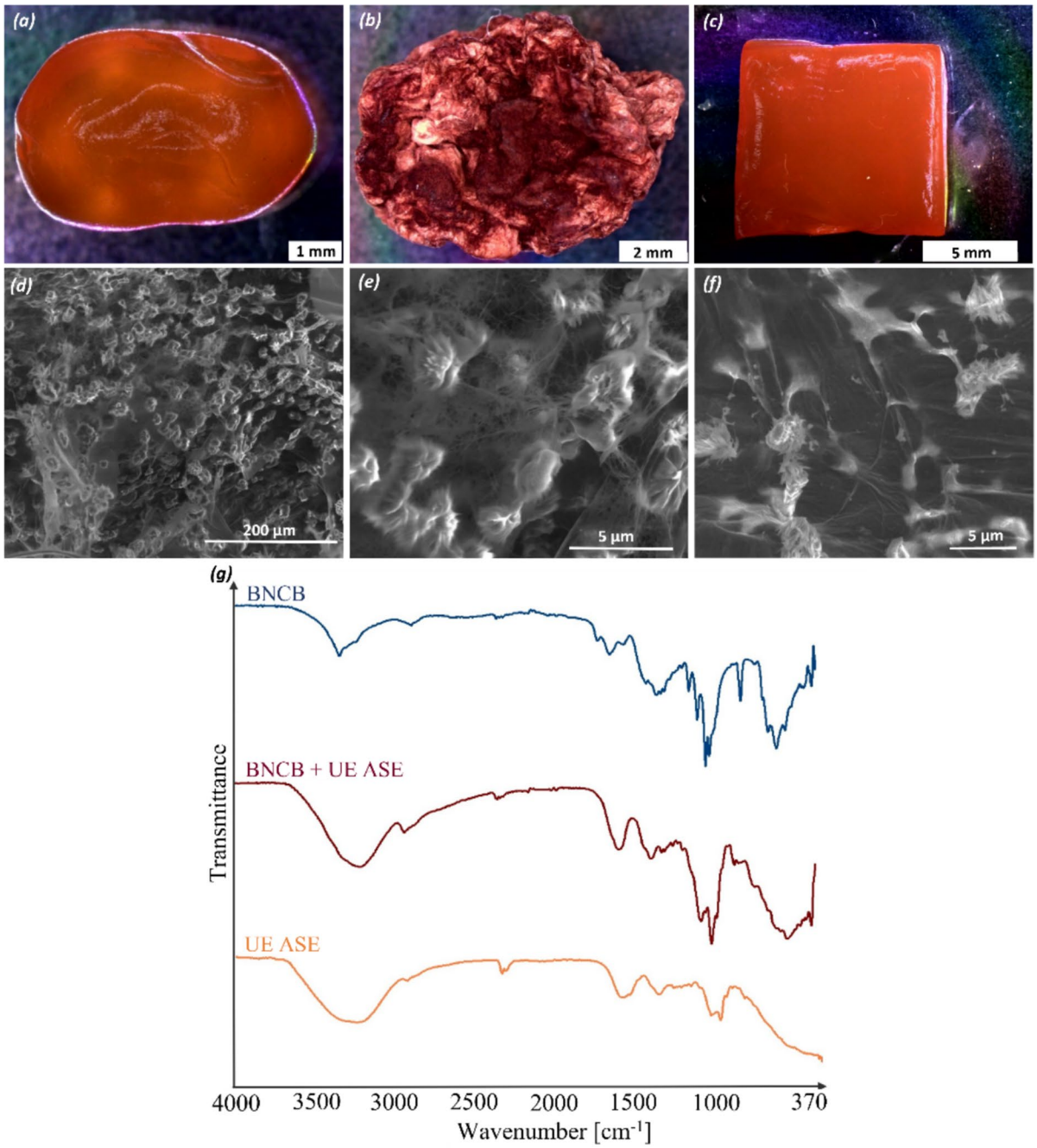

Fig. 6 Stereo microscopy imaging of **a** wet and **b** freeze-dried BNCBs and **c** wet BNCM enriched with 10 wt% UE ASE with SEM micrographs of freeze-dried BNCB + UE ASE **d, e** surface (voltage 15.0 kV, magnification 500 × and 10000x) and **f** freeze-dried BNCM + UE ASE surface (voltage 15.0 kV, magnification 500×) with corresponding **g** ATR-FTIR spectra of pure BNCB, BNCB + UE ASE and UE ASE

For example, the C = O and C = C vibrations and aromatic ring deformations bands located at around 1600 cm^{-1} (Oliveira et al. 2016) and –OH vibration of flavonoids and C–C–O groups of phenolic compounds bands around 1280 cm^{-1} (Neves et al. 2022). Characteristic bands for avocado seed compounds in

extracts are around 3340 cm^{-1} for –OH stretching, around 2930 cm^{-1} for H–C–H stretching, while the bands in the range of 1360–1315 cm^{-1} and at approx. 1030 cm^{-1} corresponding to N = O, C–C–N, and C–N stretching (Bogireddy and Agarwal 2019).

BNC generally has the ability to bind active ingredients via physical or chemical interactions. Due to its many hydroxy groups, it can interact with active ingredients through hydrogen bonding or electrostatic interactions (Jantarat et al. 2020). The spectrophotometric method determined that BNCBs can encapsulate (see Table 1) up to 72.89 ± 3.42 mg of UE ASE per one BNCB, respectively. Additionally, up to 46.61 ± 1.54 mg of UE ASE was incorporated into approximately 1 cm^2 of BNCM. It was observed that a higher concentration of UE ASE was adsorbed into wet BNCMs/BNCBs than beforehand freeze-dried BNCMs/BNCBs, which is due to the additional step of rehydration and due to the irreversibility of drying, the adsorption capacity of BNC cannot be fully recovered (Andree et al. 2021).

Antibacterial activity, release kinetics, and cytotoxicity of UE ASE from BNCMs/BNCBs

In order to evaluate the antibacterial activity of UE ASE enriched BNCMs/BNCBs from *K. xylinus* against *E. coli* and *S. aureus* the qualitative agar diffusion method was applied, and the results are presented in Table 1 and Fig. 7 (Representative results for *E. coli,* similar trends observed for *S. aureus).*

W-wet, F.D-freeze-dried, L-large (7 mm), M-medium (5 mm), S-small (2 mm). Different letters in the same column indicate significant difference ($p < 0.05$).

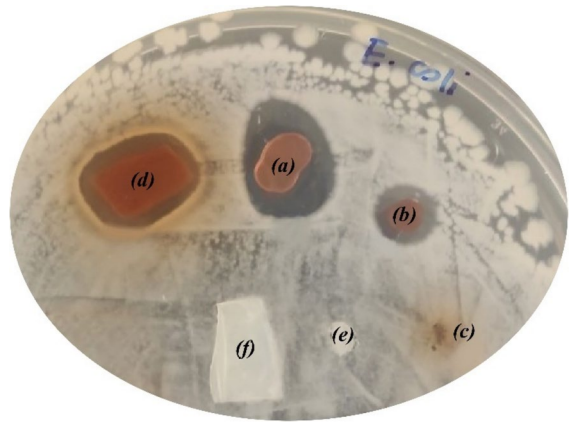

Fig. 7 Inhibition zones against *E. coli* by **a** W/BNCB-L, **b** W/BNCB-M, **c** W/BNCB-S, **d** W/BNCM enriched with 10 wt% of UE ASE. Pure **e** BNCB and **f** BNCM were applied as negative control

The growth of both tested bacteria was inhibited by BNCBs and BNCMs modified with UE ASE. The zone of inhibition was larger in the case of larger BNCBs (BNCB-L > BNCB-M), while the smallest BNCBs (BNCB-S) did not show the reduction of *E. coli* and *S. aureus* growth, due to insufficient ASE incorporation and subsequent limited release/diffusion to achieve minimum inhibitory concentrations. The antibacterial activity depends on ASE release from the BNC matrix, diffusion through the agar medium, solubility, wettability, and maintenance of effective concentrations at the bacterial interface. As expected, wet BNCMs/BNCBs (W/BNCBs and W/BNCMs) inhibited the growth of bacteria more effectively than freeze-dried BNCMs/BNCBs (F.D/

Table 1 Release of UE ASE from BNCMs/BNCBs enriched with 10 wt% UE ASE and antibacterial activity of UE ASE enriched BNCMs/BNCBs

BNCM/BNCB enriched with 10 wt% UE ASE	Incorporation of UE ASE [mg/1 BNCB or 1 cm^2 BNCM]	Release of UE ASE [%]		Inhibition zone [mm]	
		1 h	48 h	*E. coli*	*S. aureus*
W/BNCB-L	72.89 ± 3.42^{d}	15.86 ± 1.29^{a}	48.08 ± 2.65^{bc}	14 ± 1^{b}	18 ± 1^{c}
F.D/BNCB-L	49.37 ± 2.24^{c}	27.57 ± 1.46^{b}	65.20 ± 3.72^{d}	7 ± 1^{a}	9 ± 1^{a}
W/BNCB-M	52.87 ± 2.78^{c}	16.47 ± 1.64^{a}	27.48 ± 3.14^{a}	8 ± 1^{a}	11 ± 1^{ab}
F.D/BNCB-M	32.7 ± 3.13^{b}	25.15 ± 2.38^{b}	36.58 ± 1.96^{ab}	–	–
W-BNCB-S	14.48 ± 1.45^{a}	30.69 ± 2.01^{bc}	43.31 ± 2.13^{bc}	–	–
F.D/BNCB-S	9.23 ± 1.69^{a}	44.69 ± 2.76^{d}	58.73 ± 2.51^{cd}	–	–
W/BNCM	46.61 ± 1.54^{c}	37.30 ± 1.35^{d}	48.79 ± 2.67^{bc}	14 ± 3^{b}	16 ± 2^{bc}
F.D/BNCM	31.46 ± 2.37^{b}	47.50 ± 1.22^{d}	54.73 ± 3.42^{c}	10 ± 2^{ab}	12 ± 1^{ab}

BNCBs and F.D/BNCMs) due to the higher concentration of incorporated extract, better contact with the agar plate and consequently better and easier release into the nutrient agar. According to the literature (Rajagopal and Walker 2017; Rojas et al. 2018), G + bacteria are more susceptible to antimicrobial agents, compared to more resistant G- bacteria which have additional outer lipopolysaccharide membranes. This is in accordance with presented results as *S. aureus* was more susceptible (inhibition zones up to 18 ± 1 mm) to the UE ASE from BNCMs/BNCBs compared to *E. coli* (inhibition zones up to 14 ± 3 mm). The antibacterial efficiency of differently extracted ASE enriched BNCMs from *K. hansenii* has been studied in our recent study (Kupnik et al. 2024), where even possible mechanisms of action for antibacterial activity of ASE were explained and interpreted. The results of BNCBs and BNCMs from *K. xylinus* are comparable to those of *K. hansenii* BNCMs (Kupnik et al. 2024) and show additional potential for antibacterial applications of the developed biohybrids. However, to the best of our knowledge, this is the first study which presents antibacterial effective BNCBs with bio-extracts for potential delivery and release of bioactive compounds recovered from food waste-biomass.

Based on the kinetic release profiles (Fig. 8) it is possible to evaluate that the initial release rate during first hour is the highest (from 4.12 ± 0.65 up to 13.61 ± 1.43 mg and from 14.94 ± 1.86 to 17.39 ± 2.56 mg for BNCBs and BNCMs, respectively), which enables immediate release of active compounds from BNCMs/BNCBs.

Normally, as more UE ASE was incorporated in BNCBs with a larger diameter (BNCB-L > BNCB-M > BNCB-S), so the concentration of released UE ASE was also the highest from BNCB-L (up to 13.61 ± 1.43 mg), followed by BNCB-M (up to 8.71 ± 0.39 mg) and then BNCB-S (up to 4.45 ± 1.02 mg). This so-called initial burst release occurs mainly due to UE ASE particles adsorbed on the external surface of BNCMs/BNCBs. The release of W/BNCB-L after 48 h was 35.04 ± 2.61 mg, while the % cumulative release amounted to 48.08%. On the other hand, after 48 h the release from F.D/BNCB-L was 32.19 ± 1.87 mg, while the total % release was 65.20%.

It can be seen from Table 1 that in the first hour up to 44.69 ± 2.76% or 47.50 ± 1.22% of UE ASE can be released from BNCBs or BNCMs, respectively. Furthermore, the remaining UE ASE adsorbed in the bulk of the BNCMs/BNCBs enables a slow and sustainable release up to the final 48 h (up to 65.20 ± 3.72% and 54.73 ± 3.42% for BNCBs and BNCMs, respectively). Release kinetics varied significantly by formulation at both 1 h ($p < 0.001$) and 48 h ($p < 0.001$). Freeze-dried materials exhibited significantly faster burst release, with F.D/BNCB-S and F.D/BNCM releasing 40–74% more extract within the first hour compared to wet equivalents ($p < 0.01$). It should be accentuated that the cumulative released concentration (mg) of the UE ASE from wet BNCMs/

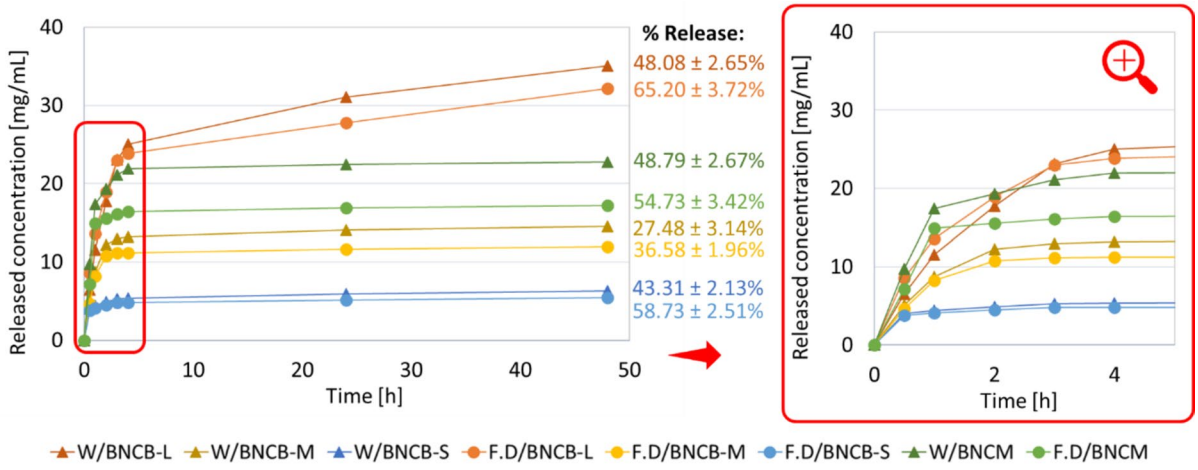

Fig. 8 Kinetics of UE ASE release from BNCBs and BNCMs (enriched with 10 wt% UE ASE) monitored at 37 ± 1 °C in 0.1 M PBS

BNCBs was higher than that of freeze-dried BNCMs/BNCBs, due to the higher adsorbed concentration of UE ASE into wet BNCMs/BNCBs, however, the percentage of the cumulative release of UE ASE from wet BNCMs/BNCBs was lower than that from freeze-dried BNCMs/BNCBs. It was reported (Mueller et al. 2014) that by using freeze-drying, BNC material can adsorb up to 70% of its original water content after re-swelling. The results of the presented study completely coincide with this phenomenon, since between 61.9 and 67.7% of the UE ASE concentration in wet BNCMs/BNCBs was incorporated into the freeze-dried BNCMs/BNCBs. During the freeze-drying process itself and thus the release of free hydroxy groups, the scission of intramolecular hydrogen bonds in the BNC structure occurs (Stanisławska et al. 2020) and the freeze-dried BNCMs/BNCBs do not have as many free sites for hydrogen bonding with UE ASE phytochemicals as wet BNCMs/BNCBs. Since the rehydration of BNC does not allow and preserves the original ability of adsorption, the BNCMs/BNCBs, that were freeze-dried in advance, adsorbed a lower amount/concentration of the UE ASE, which was most likely bound more superficially into BNC and was therefore easier released to a greater extent, which results in a higher % cumulative release. On the contrary, during adsorption with wet BNCMs/BNCBs, an exchange of water with UE ASE occurred, and therefore more UE ASE was incorporated in concentration, but it was more difficult to release, due to better UE ASE binding capacity, electrostatic interactions and hydrogen bonding, for that reason a lower % cumulative release. However, the highest total concentration of UE ASE was released from wet BNCMs/BNCBs which is in favor and in accordance with antibacterial activity of developed BNCMs/BNCBs.

The release of bioactive compounds from a polymer matrix, such as BNC, can be governed by various mechanisms (e.g., diffusion, swelling, disruption, or a combination of these) (Abasalizadeh et al. 2020). To understand the release kinetics of incorporated UE ASE from BNCMs/BNCBs in PBS, three mathematical kinetic models were applied to the experimental data. The most appropriate kinetic model was identified based on the coefficient of determination (R^2), with results summarized in Table 2.

The findings suggest that the release of UE ASE from BNCMs/BNCBs is best described by the first-order model, as it had the R^2 value closest to 1 for BNCBs-L, BNCMs-M, and BNCMs, indicating a concentration-dependent release typical for soluble compounds incorporated in porous systems. For BNCBs-S, Korsmeyer-Peppas model is determined as the most appropriate release model, describing drug release from polymeric systems where the release mechanism is not clearly known or where multiple types of release phenomena are involved. The release exponent n helps predict the drug release mechanism. If n is ≤ 0.45, it indicates Fickian diffusion; if $0.45 < n < 0.85$, it suggests non-Fickian transport (combination of diffusion and polymer relaxation); if $n = 0.89$, it belongs to Case II transport (polymer relaxation or erosion-controlled release); and if $n > 0.89$, it indicates Super Case II transport (solvent diffusion rate is higher than the rate of polymer relaxation), particularly for spherical geometries like BNCBs. For all BNCBs and BNCMs the diffusion coefficient n was < 0.45, indicating Fickian diffusion, case of diffusion-controlled release. The difference in the most appropriate release model between large/medium BNCBs (BNCBs-L/BNCBs-M) and small BNCBs (BNCBs-S) can be attributed to their surface

Table 2 Experimental data fitted to three mathematical kinetic models in order to determine the behavior and mechanism of the release kinetics of ASE from BNCMs/BNCBs

	Zero order model		First order model		Korsmeyer-Peppas model		
	R^2	k [% h^{-1}]	R^2	k [h^{-1}]	R^2	k [h^{-n}]	n [/]
W/BNCB-L	0.635	0.622	0.984	0.395	0.863	19.909	0.241
F.D/BNCMB-L	0.616	0.720	0.950	0.538	0.853	31.409	0.197
W/BNCB-M	0.328	0.206	0.990	0.940	0.638	17.953	0.131
F.D/BNCB-M	0.257	0.227	0.987	1.140	0.560	25.829	0.110
W/BNCB-S	0.682	0.247	0.603	2.158	0.942	31.563	0.086
F.D/BNCB-S	0.604	0.267	0.656	2.509	0.894	45.800	0.068
W/BNCM	0.265	0.282	0.965	1.280	0.578	35.546	0.102
F.D/BNCM	0.195	0.274	0.901	1.477	0.460	41.521	0.090

R^2-coefficient of determination, k-the release constant, n-the release exponent

area-to-volume ratio and encapsulation efficiency. Large and medium BNCBs have a lower surface area-to-volume ratio, resulting in a more uniform release rate that fits the first-order model. They also encapsulate the drug more efficiently, leading to a predictable release pattern. In contrast, small BNCBs have a higher surface area-to-volume ratio and lower encapsulation efficiency, resulting in more complex release dynamics that are better described by the Korsmeyer-Peppas model.

For further applications related to the release of UE ASE from BNC biohybrids as a potential antibacterial agent it is very important to correlate the release profile of the UE ASE with established Minimum Inhibitory Concentration (MIC) values. Results from previous study (Kupnik et al. 2023), determined by standard broth microdilution method, indicate that MIC values for UE ASE on *E. coli* and *S. aureus* are 0.21 in 2.8 mg/mL. Even the smallest wet and freeze-dried BNCB-S, which have incorporated the lowest concentration of UE ASE, already in the first hour of release (4.45 ± 1.02 and 4.12 ± 0.65 mg) exceed the MIC value by an average of 20 times in the case of *E. coli* and by 2 times in the case of *S. aureus*, while the remaining BNCMs/BNCBs exceed the MIC values by up to 82 times in the first hour of release and therefore enables exceptional antibacterial activity. In this context, BNCMs/BNCBs with incorporated UE ASE from *K. xylinus* are extremely promising release system, due to the mere high level of UE ASE incorporation and the outstanding immediate and sustained release.

The cytotoxicity of the UE ASE incorporated into BNCB/BNCM was examined with the aim of assessing its safety and biocompatibility for potential use in medical, pharmaceutical, or cosmetic applications, such as wound dressings (BNCM) or functional food (BNCB).

Cytotoxicity is a key parameter in the development of materials intended for contact with cells, as it must be ensured that the extract does not cause harmful effects on human cells, which is crucial for safe use in a clinical environment. In the case of UE ASE, cytotoxicity analyses (Fig. 9) on the THP-1 monocyte line showed that concentrations up to 300 µg/mL were not cytotoxic, as they did not reduce cell viability/metabolic activity. This indicates that these concentrations are safe for use and do not cause harmful effects on cells. However, further studies (e.g., MTT assays) are needed to confirm the safety of these concentrations in other cell types and under different experimental conditions.

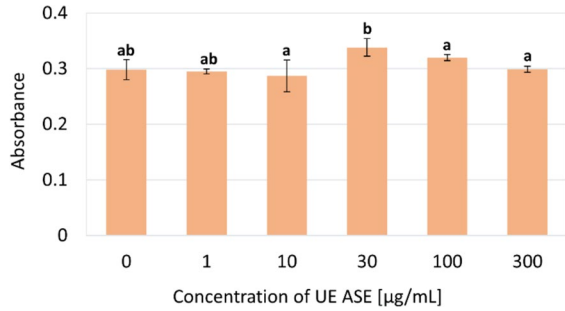

Fig. 9 Results of the cytotoxicity evaluation study on THP-1 monocyte cell line. Absorbance values represent the metabolic activity of THP-1 cells. Higher absorbance values indicate greater cell viability and metabolic activity, while lower values suggest reduced viability or cytotoxic effects. The results are presented as the mean value of triplicates with SD. Different letters above columns denote significant differences ($p < 0.05$)

ASE contains various bioactive compounds, such as polyphenols and flavonoids, which may protect cells from damage. However, cytotoxicity analyses at higher concentrations were not performed because the intense coloration of the extract itself affected the coloration of the final product, thereby interfering with the results, preventing an accurate assessment of cytotoxicity at higher concentrations. This limits a complete picture of the potential cytotoxic effects at higher concentrations.

Based on the findings of low cytotoxicity of UE ASE at concentrations up to 300 µg/mL and considering its potential due to the presence of bioactive compounds such as polyphenols and flavonoids, UE ASE has promising potential for development as an antimicrobial agent. Its relatively safe use and potential effectiveness in managing microbial infections open doors for further research and applications in medical products such as wound dressings, cosmetics, antimicrobial materials, and functional food. Among the research priorities, comprehensive long-term stability studies of such BNC biohybrids under diverse storage conditions are particularly important to support their successful commercial translation in the food and cosmetic industries. Furthermore, to contextualize our findings within the broader research landscape, Table 3 presents a comparative analysis of our BNC biohybrids with previously reported systems

using *Komagataeibacter* spp. for bioactive compound delivery.

Our study demonstrates several distinctive advantages over existing BNC biohybrid systems. The encapsulation capacity achieved (72.89 mg/bead; 46.61 mg/cm^2 membrane) substantially exceeds that reported by Osorio et al. (Osorio et al. 2024) for *V. meridionale* extract (2.91 mg/g sphere) and Kamal et al. (Kamal et al. 2022) for *D. serrulata* extract (22% attachment). While Osorio and colleagues (Osorio et al. 2024)recently pioneered plant extract-loaded BNC spheres, their study focused exclusively on cancer chemoprevention without evaluating antibacterial properties. The controlled biphasic release profile of our BNCMs/BNCBs (up to 65.20% over 48 h) offers critical advantages over systems exhibiting rapid, complete release. Adepu & Khandelwal (Adepu and Khandelwal 2020) reported 100% diclofenac sodium release within 8 h, and Lazarini (Lazarini et al. 2022) achieved 93% rifampicin release within 120 min, both lacking the sustained release necessary for prolonged antibacterial action. Our moderate release pattern enables both immediate and sustained therapeutic effects, crucial for wound dressings and infection control applications. This profile is comparable to research from Sukhtezari (Sukhtezari et al. 2017), which achieved 68% release over 66 h using β-cyclodextrin complexation, though without antibacterial evaluation. Compared to other plant extract systems, our study provides more comprehensive characterization. While Bodea et al. (Bodea et al. 2022) demonstrated broad antimicrobial activity with herbal extracts, they did not quantify encapsulation or release kinetics. Kamal and colleagues (Kamal et al. 2022) showed antibacterial activity but lacked release profile data. Our work represents the first comprehensive study of antibacterial plant extract-loaded BNC biohybrids with complete characterization: quantified encapsulation capacity, controlled biphasic release kinetics, dual-spectrum antibacterial efficacy against *S. aureus* and *E. coli*, and demonstrated biocompatibility. This combination positions these ASE-loaded biohybrids as superior alternatives to synthetic antibiotic delivery systems, particularly relevant for addressing antimicrobial resistance with natural therapeutic agents.

Table 3 Comparison of BNC biohybrids from *Komagataeibacter* spp. for bioactive compound delivery

Study	Strain	BNC form	Bioactive compound	Encapsulation capacity	Release profile	Antibacterial activity
Present study	*K. xylinus* DSM 2325	Membranes & beads	Avocado seed extract	72.89 mg/bead; 46.61 mg/cm^2 membrane	Up to 65.20% (48 h)	*E. coli, S. aureus*
(Osorio et al. 2024)	*K. medellinensis*	Beads	*Vaccinium meridionale* extract	2.91 mg/g of sphere	Up to 72% (10 min), 93% (120 min)	Not tested
(Lazarini et al. 2022)	*K. hansenii* ATCC 23769	Beads	Rifampicin	400 µg/sphere	70–100% (96 h)	*S. aureus*
(Kamal et al. 2022)	*K. hansenii*	Sheets	*Dracaena serrulata* extract	22% extract attachment to the BNC matrix	Not tested	*E. coli, S. aureus*
(Bodea et al. 2022)	*K. xylinus* ATCC 700178	Membranes/ Films	Herbal (rosemary, oregano, parsley, lovage) extracts	Not reported	Not tested	*E. coli, S. aureus, C. albicans*
(Adepu and Khandelwal 2020)	*K hansenii* ATCC 23769	Membranes	Diclofenac sodium	2.3 mg/cm^2	Up to 100% (8 h)	Not tested
(Sukhtezari et al. 2017)	*K. xylinus*	Films	*Scrophularia striata* Boiss. extract + β-cyclodextrin	5 wt% of film dry base	Up to 68% (66 h)	Not tested

Conclusions

The results of the presented study showed that both, selection of bacterial strain and cultivation conditions, have a significant impact on BNC productivity, properties and quality. Regarding the static conditions and obtaining BNCMs, *K. xylinus* provided faster (3 days) and higher (up to 518.4 g/L) BNCMs productivity with a bit higher C_I (80.56%), compared to *K. hansenii* (17–21 days, up to 117.8 g/L, 78.64%). Furthermore, the production of BNCBs was only possible with *K. xylinus*, with slightly reduced productivity under dynamic conditions (76.8 g/L) compared to the static ones (81.0 g/L) after 3 days and 10% (v/v) of added inoculum.

Our study demonstrates that biohybrids composed of BNC from *K. xylinus* and UE ASE were developed in the form of membranes and beads, exhibiting antibacterial activity and representing promising drug release systems. The UE ASE was incorporated into BNCMs/BNCBs under a feasible and simple process and demonstrated antibacterial potential against *E. coli* and *S. aureus*. The BNCMs/BNCBs modified with UE ASE demonstrated viability for adsorption of high concentrations of UE ASE (up to 72.89 mg/one BNCB and up to 46.61 mg/1 cm^2 of BNCM). The developed biohybrids represent a synergistic system, where BNC enables an optimal UE ASE desorption kinetic profile, allowing for both, immediate (up to 17.39 mg in 1 h) and sustained (up to 35.04 mg) release of antibacterial avocado seed compounds. This, combined with the low cytotoxicity of UE ASE at concentrations up to 300 µg/mL, highlights the potential of these biohybrids for applications in cosmetics, functional food, drug delivery, and medical products such as wound dressings and antimicrobial materials.

Author contributions Conceptualization, M. L., M.P. and K.K.; methodology, M.P. and K.K; formal analysis, K.K.; cytotoxicity analysis, N.B.; data curation, K.K..; writing—original draft preparation, K.K..; writing—review, M.L., M.P.; writing—editing, K.K.; visualization, K.K..; supervision, M.L. and M.P.; funding acquisition, M.L. and Z.K. All the authors have read and approved the final version of the manuscript.

Funding This research was supported by the Slovenian Research and Innovation Agency (ARIS) within the frame of Program P2-0046 (Separation Processes and Production Design), P2-0424 (Design of novel nano/material properties & applications), L2-4430 (Production, Isolation and Formulation of Health Beneficial Substances from*Helichrysum italicumfor Applications in the Cosmetic Industry), and Young Researcher ARIS Fellowship Contract No. 2187/FS-2019. The authors acknowledge the use of research equipment for the production of biological substances and their detection, procured within the Project "Upgrading national research infrastructures—RIUM", which was co-financed by the Republic of Slovenia, the Ministry of Higher Education, Science and Innovation, and the European Union from the European Regional Development Fund, and the system of downstream processes for performance of obtaining biological substances (Package 21, ARIS).*

Data availability No datasets were generated or analysed during the current study.

Declarations

Conflict of interests The authors declare no competing interests.

Ethical approval This study does not include any studies conducted by any author on human participants or animals. The authors claim compliance with the ethical standards.

References

Abasalizadeh F, Moghaddam SV, Alizadeh E, akbari E, Kashani E, Fazljou SMB, Torbati M, Akbarzadeh A (2020) Alginate-based hydrogels as drug delivery vehicles in cancer treatment and their applications in wound dressing and 3D bioprinting. J Biol Eng 14(1):8. https://doi.org/10.1186/s13036-020-0227-7

Adepu S, Khandelwal M (2020) Ex-situ modification of bacterial cellulose for immediate and sustained drug release with insights into release mechanism. Carbohydr Polym 249:116816. https://doi.org/10.1016/j.carbpol.2020.116816

Andree V, Niopek D, Müller C, Eiselt J-P, Foh N, Rzany A, Hensel B (2021) Influence of drying methods on the physical properties of bacterial nanocellulose. Mater Res Express 8(2):025402. https://doi.org/10.1088/2053-1591/abe016

Atalla RH, VanderHart DL (1984) Native cellulose: a composite of two distinct crystalline forms. Science 223(4633):283–285. https://doi.org/10.1126/science.223.4633.283

Atykyan N, Revin V, Shutova V (2020) Raman and FT-IR spectroscopy investigation the cellulose structural differences from bacteria *Gluconacetobacter sucrofermentans* during the different regimes of cultivation on a molasses media. AMB Express 10(1):84. https://doi.org/10.1186/s13568-020-01020-8

Azeredo HMC, Barud H, Farinas CS, Vasconcellos VM, Claro AM (2019) Bacterial Cellulose as a Raw Material for Food and Food Packaging Applications. Front Sustain Food Syst 3. https://doi.org/10.3389/fsufs.2019.00007

Bae S, Sugano Y, Shoda M (2004) Improvement of bacterial cellulose production by addition of agar in a jar fermentor. J Biosci Bioeng 97(1):33–38. https://doi.org/10.1016/S1389-1723(04)70162-0

Bodea IM, Cătunescu GM, Pop CR, Fiț NI, David AP, Dudescu MC, Stănilă A, Rotar AM, Beteg FI (2022) Antimicrobial properties of bacterial cellulose films enriched with bioactive herbal extracts obtained by microwave-assisted extraction. Polymers 14(7):1435. https://doi.org/10.3390/polym14071435

Bogireddy N, Agarwal V (2019) *Persea americana* seed extract mediated gold nanoparticles for mercury(II)/iron(III) sensing, 4- nitrophenol reduction, and organic dye degradation. RSC Adv 9:39834. https://doi.org/10.1039/c9ra08233f

Chen G, Chen L, Wang W, Chen S, Wang H, Wei Y, Hong FF (2019a) Improved bacterial nanocellulose production from glucose without the loss of quality by evaluating thirteen agitator configurations at low speed. Microb Biotechnol 12(6):1387–1402. https://doi.org/10.1111/1751-7915.13477

Chen G, Wu G, Chen L, Wang W, Hong FF, Jönsson LJ (2019b) Performance of nanocellulose-producing bacterial strains in static and agitated cultures with different starting pH. Carbohydr Polym 215:280–288. https://doi.org/10.1016/j.carbpol.2019.03.080

Dabas D, Elias RJ, Lambert JD, Ziegler GR (2011) A colored avocado seed extract as a potential natural colorant. J Food Sci 76(9):C1335–C1341. https://doi.org/10.1111/j.1750-3841.2011.02415.x

Dayal MS, Goswami N, Sahai A, Jain V, Mathur G, Mathur A (2013) Effect of media components on cell growth and bacterial cellulose production from *Acetobacter aceti* MTCC 2623. Carbohydr Polym 94(1):12–16. https://doi.org/10.1016/j.carbpol.2013.01.018

Digel I, Akimbekov N, Rogachev E, Pogorelova N (2023) Bacterial cellulose produced by *Medusomyces gisevii* on glucose and sucrose: biosynthesis and structural properties. Cellulose 30(18):11439–11453. https://doi.org/10.1007/s10570-023-05592-z

Fontana JD, Koop HS, Tiboni M, Grzybowski A, Pereira A, Kruger CD, da Silva MGR, Wielewski LP (2017) Chapter 7 - New Insights on Bacterial Cellulose. In: Grumezescu AM, Holban AM (eds) Food Biosynthesis. Academic Press, pp 213–249

French AD (2014) Idealized powder diffraction patterns for cellulose polymorphs. Cellulose 21(2):885–896. https://doi.org/10.1007/s10570-013-0030-4

French AD, Santiago Cintrón M (2013) Cellulose polymorphy, crystallite size, and the Segal Crystallinity Index. Cellulose 20(1):583–588. https://doi.org/10.1007/s10570-012-9833-y

Gama M, Dourado F, Bielecki S (2016) Bacterial Nanocellulose: From Biotechnology to Bio-Economy. Elsevier

Gayathri G, Srinikethan G (2019) Bacterial cellulose production by *K. saccharivorans* BC1 strain using crude distillery effluent as cheap and cost effective nutrient medium. Int J Biol Macromol. https://doi.org/10.1016/j.ijbiomac.2019.07.159

Ghozali M, Meliana Y, Chalid M (2021) Synthesis and characterization of bacterial cellulose by *Acetobacter xylinum* using liquid tapioca waste. Mater Today Proc 44:2131–2134. https://doi.org/10.1016/j.matpr.2020.12.274

Gupte Y, Kulkarni A, Raut B, Sarkar P, Choudhury R, Chawande A, Kumar GRK, Bhadra B, Satapathy A, Das G, Vishnupriya B, Dasgupta S (2021) Characterization of nanocellulose production by strains of *Komagataeibacter* sp. isolated from organic waste and Kombucha. Carbohydr Polym 266:118176. https://doi.org/10.1016/j.carbpol.2021.118176

Heydorn RL, Lammers D, Gottschling M, Dohnt K (2023) Effect of food industry by-products on bacterial cellulose production and its structural properties. Cellulose 30(7):4159–4179. https://doi.org/10.1007/s10570-023-05097-9

Hu W, Chen S, Yang J, Li Z, Wang H (2014) Functionalized bacterial cellulose derivatives and nanocomposites. Carbohydr Polym 101:1043–1060. https://doi.org/10.1016/j.carbpol.2013.09.102

Jantarat C, Attakitmongkol K, Nichsapa S, Sirathanarun P, Srivaro S (2020) Molecularly imprinted bacterial cellulose for sustained-release delivery of quercetin. J Biomater Sci Polym Ed 31(15):1961–1976. https://doi.org/10.1080/09205063.2020.1787602

Kamal T, Ul-Islam M, Khan SB, Bakhsh EM, Chani MTS (2022) Development of plant extract impregnated bacterial cellulose as a green antimicrobial composite for potential biomedical applications. Ind Crops Prod 187:115337. https://doi.org/10.1016/j.indcrop.2022.115337

Klemm D, Kramer F, Moritz S, Lindström T, Ankerfors M, Gray D, Dorris A (2011) Nanocelluloses: a new family of nature-based materials. Angew Chem Int Ed Engl 50(24):5438–5466. https://doi.org/10.1002/anie.201001273

Konczak I, Zhang W (2004) Anthocyanins - more than nature's colours. J Biomed Biotechnol 2004(5):239–240. https://doi.org/10.1155/S1110724304407013

Kučuk N, Primožič M, Knez Ž, Leitgeb M (2024) Alginate beads with encapsulated bioactive substances from *Mangifera indica* peels as promising peroral delivery systems. Foods 13(15):2404. https://doi.org/10.3390/foods13152404

Kupnik K, Primožič M, Kokol V, Leitgeb M (2020) Nanocellulose in drug delivery and antimicrobially active materials. Polymers 12(12):2825. https://doi.org/10.3390/polym12122825

Kupnik K, Primožič M, Kokol V, Knez Ž, Leitgeb M (2023) Enzymatic, antioxidant, and antimicrobial activities of bioactive compounds from avocado (*Persea americana* L.) seeds. Plants 12(5):1201. https://doi.org/10.3390/plants12051201

Kupnik K, Primožič M, Kokol V, Knez Ž, Leitgeb M (2024) Antibacterial *Komagataeibacter hansenii* nanocellulose membranes with avocado seed bioactive compounds. Cellulose. https://doi.org/10.1007/s10570-024-05839-3

Lazarini SC, Yamada C, da Nóbrega TR, Lustri WR (2022) Production of sphere-like bacterial cellulose in cultivation media with different carbon sources: a promising sustained release system of rifampicin. Cellulose 29(11):6077–6092. https://doi.org/10.1007/s10570-022-04644-0

Lee K-Y, Buldum G, Mantalaris A, Bismarck A (2014) More than meets the eye in bacterial cellulose: biosynthesis, bioprocessing, and applications in advanced fiber composites. Macromol Biosci 14(1):10–32. https://doi.org/10.1002/mabi.201300298

Manoukian OS, Sardashti N, Stedman T, Gailiunas K, Ojha A, Penalosa A, Mancuso C, Hobert M, Kumbar SG (2019) Biomaterials for Tissue Engineering and Regenerative Medicine. In: Narayan R (ed) Encyclopedia of Biomedical Engineering. Elsevier, Oxford, pp 462–482

Mohite BV, Patil SV (2014) Bacterial cellulose of *Gluconoacetobacter hansenii* as a potential bioadsorption agent for its green environment applications. J Biomater Sci Polym Ed 25(18):2053–2065. https://doi.org/10.1080/09205063.2014.970063

Mueller A, Zink M, Hessler N, Wesarg F, Mueller FA, Kralisch D, Fischer D (2014) Bacterial nanocellulose with a shape-memory effect as potential drug delivery system. RSC Adv 4(100):57173–57184. https://doi.org/10.1039/c4ra09898f

Neves EZ, Kumineck Junior SR, Katrucha GP, Silveira VF, Silveira MLL, Pezzin APT, Schneider ALdosS, Garcia MCF, Apati GP (2022) Development of bacterial cellulose membranes incorporated with plant extracts. Macromol Symp 406(1):2200031. https://doi.org/10.1002/masy.202200031

Oliveira RN, Mancini MC, Oliveira FCSde, Passos TM, Quilty B, Thiré RMdaSM, McGuinness GB (2016) FTIR analysis and quantification of phenols and flavonoids of five commercially available plants extracts used in wound healing. Materia Rio J 21:767–779. https://doi.org/10.1590/S1517-707620160003.0072

Osorio M, Martinez E, Kooten TV, Gañán P, Naranjo T, Ortiz I, Castro C (2020) Biomimetics of microducts in three-dimensional bacterial nanocellulose biomaterials for soft tissue regenerative medicine. Cellulose 27(10):5923–5937. https://doi.org/10.1007/s10570-020-03175-w

Osorio M, Posada L, Martínez E, Estrada V, Quintana G, Maldonado ME, Peresin S, Orozco J, Castro C (2024) Bacterial nanocellulose spheres coated with meta acrylic copolymer: *Vaccinium meridionale swartz* extract delivery for colorectal cancer chemoprevention. Food Hydrocoll 147:109310. https://doi.org/10.1016/j.foodhyd.2023.109310

Pötzinger Y, Kralisch D, Fischer D (2017) Bacterial nanocellulose: the future of controlled drug delivery? Ther Deliv 8(9):753–761. https://doi.org/10.4155/tde-2017-0059

Rajagopal M, Walker S (2017) Envelope structures of gram-positive bacteria. Curr Top Microbiol Immunol 404:1–44. https://doi.org/10.1007/82_2015_5021

Rojas ER, Billings G, Odermatt PD, Auer GK, Zhu L, Miguel A, Chang F, Weibel DB, Theriot JA, Huang KC (2018) The outer membrane is an essential load-bearing element in Gram-negative bacteria. Nature 559(7715):617–621. https://doi.org/10.1038/s41586-018-0344-3

Sakthivel K, Periyasamy S, Hungund B (2016) Biosynthesis of bacterial cellulose and imparting antibacterial property through novel bio-agents. Res J Biotechnol 11(9):86–93

Segal L, Creely JJ, Martin AE, Conrad CM (1959) An empirical method for estimating the degree of crystallinity of native cellulose using the X-ray diffractometer. Text Res J 29(10):786–794. https://doi.org/10.1177/004051755902901003

Sharma C, Bhardwaj NK (2019) Bacterial nanocellulose: present status, biomedical applications and future perspectives. Mater Sci Eng C Mater Biol Appl 104:109963. https://doi.org/10.1016/j.msec.2019.109963

Shavyrkina NA, Budaeva VV, Skiba EA, Mironova GF, Bychin NV, Gismatulina YA, Kashcheyeva EI, Sitnikova AE, Shilov AI, Kuznetsov PS, Sakovich GV (2021) Scale-up of biosynthesis process of bacterial nanocellulose. Polymers 13(12):1920. https://doi.org/10.3390/polym13121920

Singhsa P, Narain R, Manuspiya H (2018) Physical structure variations of bacterial cellulose produced by different *Komagataeibacter xylinus* strains and carbon sources in static and agitated conditions. Cellulose 25(3):1571–1581. https://doi.org/10.1007/s10570-018-1699-1

Stanisławska A, Staroszczyk H, Szkodo M (2020) The effect of dehydration/rehydration of bacterial nanocellulose on its tensile strength and physicochemical properties. Carbohydr Polym 236:116023. https://doi.org/10.1016/j.carbpol.2020.116023

Sukhtezari S, Almasi H, Pirsa S, Zandi M, Pirouzifard M (2017) Development of bacterial cellulose based slow-release active films by incorporation of *Scrophularia striata* Boiss. extract. Carbohydr Polym 156:340–350. https://doi.org/10.1016/j.carbpol.2016.09.058

Tantratian S, Tammarate P, Krusong W, Bhattarakosol P, Phunsri A (2005) Effect of Dissolved Oxygen on Cellulose Production by Acetobacter sp. J Sci Res Chula Univ 30

Thakkar S, Misra M (2017) Electrospun polymeric nanofibers: new horizons in drug delivery. Eur J Pharm Sci 107:148–167. https://doi.org/10.1016/j.ejps.2017.07.001

Urbina L, Corcuera MÁ, Gabilondo N, Eceiza A, Retegi A (2021) A review of bacterial cellulose: sustainable production from agricultural waste and applications in various fields. Cellulose 28(13):8229–8253. https://doi.org/10.1007/s10570-021-04020-4

Vigentini I, Fabrizio V, Dellacà F, Rossi S, Azario I, Mondin C, Benaglia M, Foschino R (2019) Set-up of bacterial cellulose production from the genus *Komagataeibacter* and its use in a gluten-free bakery product as a case study. Front Microbiol 10:1953. https://doi.org/10.3389/fmicb.2019.01953

Wada M, Okano T, Sugiyama J (2001) Allomorphs of native crystalline cellulose I evaluated by two equatorial

d-spacings. J Wood Sci 47(2):124–128. https://doi.org/10.1007/BF00780560

Wang J, Tavakoli J, Tang Y (2019) Bacterial cellulose production, properties and applications with different culture methods – a review. Carbohydr Polym 219:63–76. https://doi.org/10.1016/j.carbpol.2019.05.008

Wu S-C, Lia Y-K (2008) Application of bacterial cellulose pellets in enzyme immobilization. J Mol Catal B Enzym 54(3):103–108. https://doi.org/10.1016/j.molcatb.2007.12.021